Hydrazone-Bearing PMMA-Functionalized Magnetic Nanocubes as pH-Responsive Drug Carriers for Remotely Targeted Cancer Therapy in Vitro and in Vivo

ARTICLE *in* ACS APPLIED MATERIALS & INTERFACES · APRIL 2014

Impact Factor: 6.72 · DOI: 10.1021/am500818m · Source: PubMed

9 AUTHORS, INCLUDING:

Xingwei Ding
Nanchang University
16 PUBLICATIONS **295** CITATIONS
SEE PROFILE

Zhong Luo
Nanyang Technological University
48 PUBLICATIONS **933** CITATIONS
SEE PROFILE

Beilu Zhang
Michigan Technological Univeristy
9 PUBLICATIONS **220** CITATIONS
SEE PROFILE

Junjie Liu
Chongqing University
12 PUBLICATIONS **126** CITATIONS
SEE PROFILE

ACS APPLIED MATERIALS & INTERFACES

Research Article

www.acsami.org

Hydrazone-Bearing PMMA-Functionalized Magnetic Nanocubes as pH-Responsive Drug Carriers for Remotely Targeted Cancer Therapy in Vitro and in Vivo

Xingwei Ding, Yun Liu, Jinghua Li, Zhong Luo, Yan Hu, Beilu Zhang, Junjie Liu, Jun Zhou, and Kaiyong Cai*

Key Laboratory of Biorheological Science and Technology, Ministry of Education, College of Bioengineering, Chongqing University, Chongqing 400044, P. R. China

Supporting Information

ABSTRACT: To develop vehicles for efficient chemotherapeutic cancer therapy, we report a remotely triggered drug delivery system based on magnetic nanocubes. The synthesized magnetic nanocubes with average edge length of around 30 nm acted as cores, whereas poly(methyl methacrylate) (PMMA) was employed as an intermediate coating layer. Hydrazide was then tailored onto PMMA both for doxorubicin (DOX) loading and pH responsive drug delivery via the breakage of hydrazine bonds. The successful fabrication of the pH responsive drug carrier was confirmed by transmission electron microscopy, Fourier transform infrared spectroscopy, thermogravimetric analysis, and magnetic hysteresis loops, respectively. The carrier was stable at neutral environment and doxorubicin released at pH of 5.0. Cell viability assay and confocal laser scanning microscopy observations demonstrated that the loaded DOX could be efficiently released after cellular endocytosis and induced cancer cells apoptosis thereby. More importantly, the carrier could be guided to the tumor tissue site with an external magnetic field and led to efficient tumor inhibition with low side effects, which were reflected by magnetic resonance imaging (MRI), change of tumor size, TUNEL staining, and H&E staining assays, respectively. All results suggest that hydrazide-tailoring PMMA-coated magnetic nanocube would be a promising pH-responsive drug carrier for remotely targeted cancer therapy in vitro and in vivo.

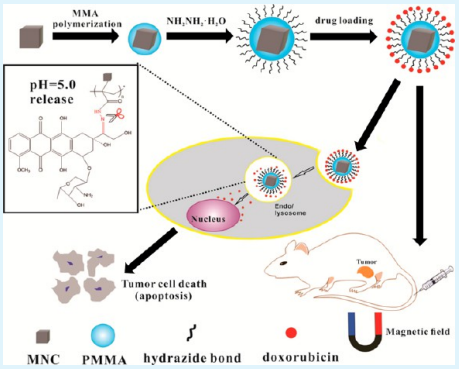

KEYWORDS: *magnetic nanocubes, pH-responsive drug delivery, cancer therapy, in vivo, cytotoxicity*

INTRODUCTION

During past decades, various nanocarriers (iron oxide magnetic nanoparticles,[1,2] mesoporous silica nanoparticles,[3,4] gold nanoparticles,[5,6] etc.) were extensively exploited to deliver chemotherapeutic agents for cancer therapy, because most administrated chemotherapeutic agents are toxic, potentially leading to severe side effects to healthy organs of a host.[7−9] For cancer therapy, nanocarriers as drug vehicles have advantage over microsized drug carriers because they could increase drug accumulation due to enhanced permeation and retention (EPR) effect at solid tumor site.[10] Magnetic nanoparticles have gained significant attention as drug delivery and imaging facilities mainly because of their good biocompatibility and intrinsic magnetic properties.[11,12] In addition, MRI is an important diagnostic tool in cancer therapy. Recently, magnetic nanocubes attract much attention for biomedical applications, such as contrast agents for MRI, mainly because of their tunable sizes, high colloidal stability in aqueous environments, and excellent r^2 relaxivity.[13−15]

To sensitively deliver drugs to a tumor tissue, researchers have designed various kinds of smart controlled drug delivery systems in responding to the signals within the microenvironment of a tumor tissue, such as pH,[16,17] temperature,[18,19] enzyme, etc.[20,21] As one of the most promising drug delivery systems, pH-responsive nanocarrier could enable on-demand drug delivery when a nanocarrier was endocytosed and distributed in endosomal/lysosomal compartments (pH 4.0−5.0) of cells at a tumor site.[16,22] Some functional moieties and polymers including hydrazine,[23] PAH/PSS,[24] PNIPAAm,[25] carboxyphenylboronic acid,[26] and peptide amphiphile[27] have been incorporated into different materials to construct pH-responsive drug delivery systems. Nevertheless, fabrication of a nanocarrier for controlled drug delivery with excellent biocompatibility, biodegradability, and long blood circulation time still needs to be investigated.

Poly(methyl methacrylate) (PMMA) was widely used in biomedical field as a nontoxic polymer. Because of its excellent biocompatibility and biodegradability, PMMA has been employed for the fabrication of drug delivery systems.[28] Nevertheless, to deliver a nanocarrier to a solid tumor with long-term blood circulation, PMMA should be decorated or incorporated with some functional moieties or hydrophilic molecules to change its hydrophobicity, such as hydrazine,[29] protein,[30] and SiO_2.[31]

Received: February 8, 2014
Accepted: April 21, 2014
Published: April 21, 2014

   dx.doi.org/10.1021/am500818m | ACS Appl. Mater. Interfaces 2014, 6, 7395−7407

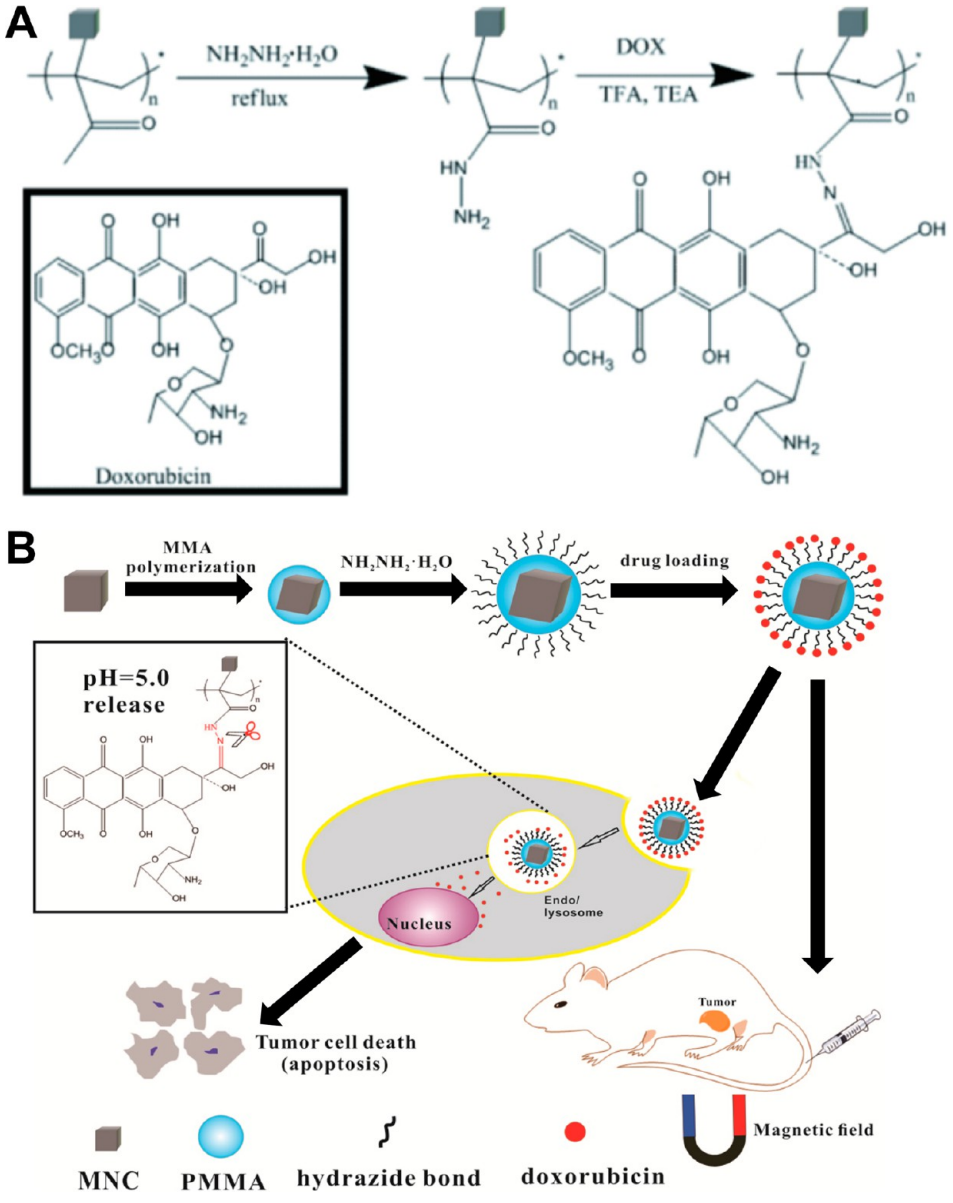

Figure 1. (A) Synthetic route of pH-responsive N-PMNCs@DOX. TFA = trifluoroaceticacid, TEA = triethylamine; and (B) Schematic illustration of the fabrication of an intracellular pH-responsive drug delivery system based on MNCs for remotely targeted tumor therapy in vitro and in vivo.

Herein, we report an approach to fabricate a pH-responsive drug delivery system based on hydrazide decorating PMMA coated magnetic FeO nanocubes (MNCs) that demonstrated great potential for controlled antitumor drug release in vitro and remotely targeted cancer therapy in vivo. Our approach involves decorating hydrazide on PMMA to transform its hydrophobicity to hydrophilicity. Furthermore, the decorated hydrazide was used to couple with antitumor drug of doxorubicin (DOX), thus yielding pH-responsive hydrazone bonds between DOX and PMMA (Figure 1 A). On the other hand, MNCs were employed as core of the drug delivery system for magnetic targeting in vivo (Figure 1 B). We hypothesized that the present system could be served as an intelligent nanocarrier for intracellular pH-responsive anticancer drug delivery in vitro and remotely targeted for tumor inhibition in vivo.

RESULTS AND DISCUSSION

To confirm our hypothesis, we first synthesized MNCs via a thermal decomposition method.[32] Next, the synthesized MNCs were coated with PMMA via an aqueous-phase radical polymerization,[33] leading to PMNCs. Subsequently, methyl bonds of PMNCs were replaced by hydrazide through a reaction with hydrazine hydrate, resulting in hydrophilic hydrazide-PMNCs (N-PMNCs) (see the Supporting Information, Figures S1 and S2). Finally, DOX was covalently attached to N-PMNCs to form pH-sensitive hydrazone bonds through the reaction between keto groups of DOX molecules and amino groups of N-PMNCs molecules (Figure 1 A), leading to DOX-loaded MNCs (N-PMNCs@DOX). Transmission electron microscopy (TEM) images showed that the synthesized MNCs had relatively uniform square feature with good dispersion property. The sizes of MNCs were defined as edge lengths of square MNCs.[14,34] The average edge lengths of MNCs were around 30 nm (Figure 2A). Compared with native MNCs, PMNCs displayed shadow layer around MNCs with thickness of around 2 nm (Figure 2 B). It suggests that MNCs was successfully coated by PMMA. After loading DOX, N-PMNCs@DOX displayed similar morphology to that of PMNCs (Figure 2 C). However, the dispersion of both

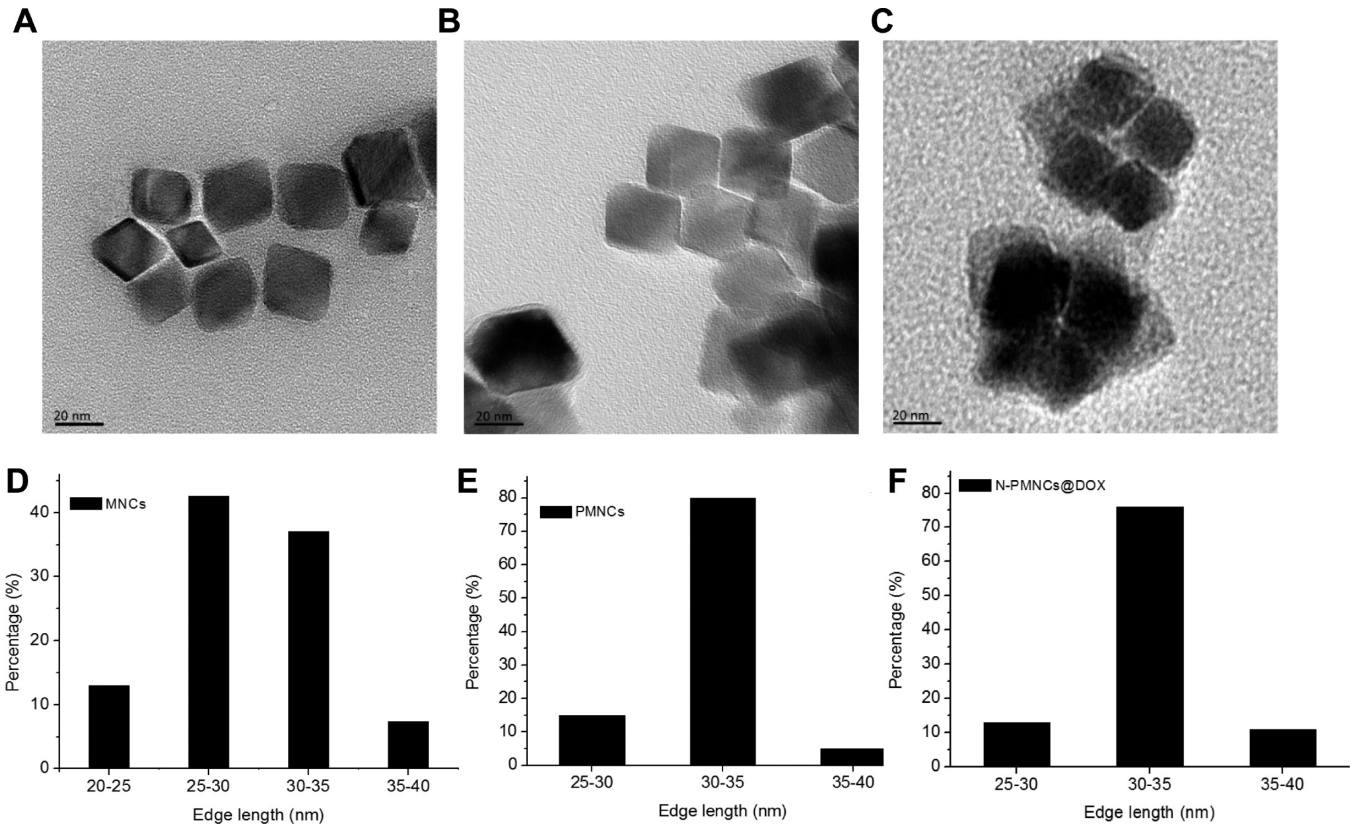

Figure 2. (A) Representative TEM image of MNCs; (B) representative TEM image of PMNCs; (C) representative TEM image of N-PMNCs@DOX (scale bar: 20 nm); and size distributions of (D) MNCs, (E) PMNCs, and (F) N-PMNCs@DOX (n = 300).

PMNCs and N-PMNCs@DOX was slightly reduced mainly due to the presence of viscous PMMA resin with large branch chains.[35] The synthesized MNCs displayed a relatively uniform edge length of 30 ± 4.1 nm (mean ± SD, n = 300) (Figure 2D). PMNCs kept uniform square feature with an average edge length of 32 ± 3 nm (mean ± SD, n = 300) and around 80% of PMNCs were distributed within the range of 30−35 nm (Figure 2E). N-PMNCs@DOX displayed an average edge length of 33 ± 3.8 nm (mean ± SD, n = 300) (Figure 2F). The trivial difference in edge lengths between N-PMNCs@DOX and PMNCs could be interpreted that DOX was only a small molecule. Thus, the coupling of DOX with PMNCs would contribute only a little to the edge length of N-PMNCs@DOX.

To monitor the fabrication process, samples were characterized by Fourier transform infrared spectroscopy (FTIR), thermogravimetric analysis (TGA) and magnetic hysteresis loops (VSM), respectively. The peak at 585 cm^{-1} was observed from the spectra of MNCs, PMNCs and N-PMNCs, which was assigned to Fe−O bonds.[32] The strong peak of the stretching vibration of C═O (1706 cm^{-1}) indicates that PMMA have been successfully coated on MNCs.[36] The new peaks appear at 1645 and 1533 cm^{-1} suggest that hydrazide have been decorated on PMMA molecules. Meanwhile, the new peak of amino group (1605 cm^{-1}) also indicates that N-PMNCs have been successfully fabricated (Figure 3A).[37] Magnetic hysteresis loops of the prepared MNCs displayed a magnetization value of 27.0 emu/g. The result was consistent with a previous study.[32] However, the magnetization value of PMNCs decreased to 17.1 emu/g. It was related to the fact that PMMA layer was coated onto the surfaces of MNCs. In addition, the magnetization value of N-PMNCs@DOX slightly decreased to 16.6 emu/g, which indicates that the loading of DOX only slightly reduced the magnetization value of drug delivery carrier (Figure 3B). To investigate the content of coated PMMA and loaded DOX in the drug delivery system, we employed TGA to quantitatively characterize the samples. PMMA and DOX were chosen as controls in this study. MNCs displayed a weight loss of about 8.4%, whereas N-PMNCs showed around 51.3% weight loss, indicating that the weight proportion of PMMA in the PMNCs was around 42.9%; whereas N-PMNCs@DOX displayed a weight loss of about 55%. The result suggests that the weight proportion of DOX in N-PMNCs@DOX was around 3.7% (Figure 3C). Calculating from eq 1,[36,38] the drug loading efficiency of N-PMNCs@DOX system was determined to be around 20.4%.

To confirm our hypothesis that N-PMNCs@DOX could efficiently control DOX release in responding to the pH change, N-PMNCs@DOX were exposed to phosphate buffered saline (PBS) with pH of 7.4 (physiological pH value) and pH of 5.0 (pH value of endosome/lysosome) at 37 °C, respectively. Only around 3.61% of DOX released from N-PMNCs@DOX at physiological condition (pH 7.4) at the initial incubation for 2 h. It suggests that N-PMNCs@DOX has good drug retaining efficiency. However, around 56% of DOX quickly released when the pH value decreased to 5.0, indicating that N-PMNCs@DOX was highly sensitive to pH stimulus. It could be interpreted that the hydrazone bonds linking with PMMA and DOX were broken down under acidic condition, leading to the release of DOX. After incubation at pH 5.0 for 40 h, around 84% of DOX released from N-PMNCs@DOX; whereas only 8.47% of DOX released when incubation at pH 7.0 (Figure 4A). It reveals that N-PMNCs@DOX could keep stable under physiological environment, while release most DOX quickly when delivered

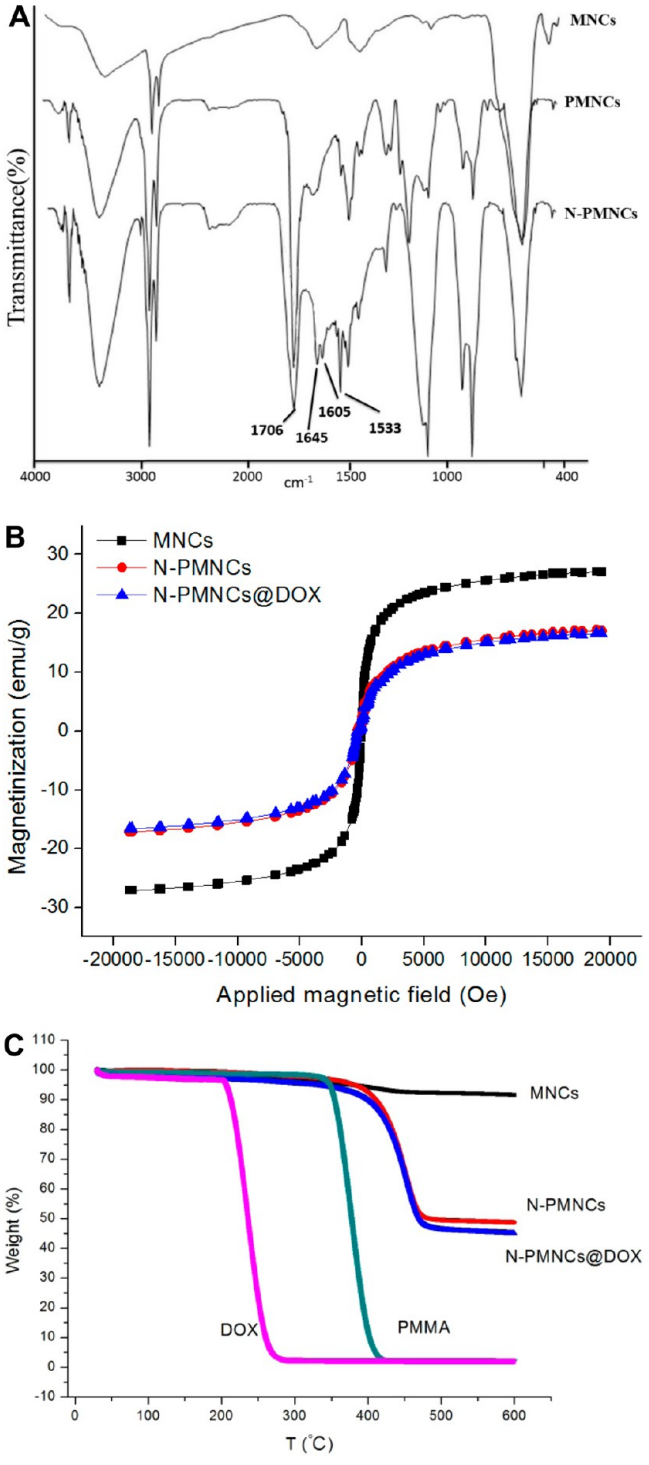

Figure 3. (A) FITR spectra of MNCs, PMNCs and N-PMNCs; (B) magnetic hysteresis loops of MNCs and N-PMNCs; and (C) TGA curves of DOX, PMMA, MNCs, N-PMNCs, and N-PMNCs@DOX, respectively.

to endosomes/lysosomes of cancer cells (pH 4.0–5.0).[16,22] To further investigate the pH-response of drug delivery system in a dynamic condition, we adjusted the pH value of the incubation solution to 5.0 when N-PMNCs@DOX were incubated with a medium of pH 7.4 for 4 h. Only 4.1% of DOX released from N-PMNCs@DOX at the initial 4 h (pH 7.4, off). However, when the pH value was adjusted to 5.0, around 35.5% of DOX released after incubation for another 6 h. Moreover, the cumulative DOX reached around 82.1% after incubation for 36 h (pH 5.0, on) (Figure 4 B). The potential mechanism lies in that hydrazone between PMMA and DOX were stable (off) at physiological condition (pH 7.4). Upon exposure to an acidic environment (pH 5.0), the hydrazone bonds were broken down, resulting in DOX release (on).

To investigate the feasibility of the N-PMNCs@DOX system for biomedical application, we performed systematic evaluations in vitro and in vivo as follows. First, we comparatively investigated the cytotoxicity of N-PMNCs, DOX and N-PMNCs@DOX. Cell viability was evaluated with cell counting assay kit-8 (CCK-8). Hela cells treated with N-PMNCs showed similar cell viability to those cultured onto tissue culture polystyrene (TCPS, control) (Figure 6 A). It suggests that N-PMNCs have good cytocompatibility. DOX displayed moderate cytotoxicity to cells, mainly because of its hydrophobic nature with relatively low solubility in cell culture medium. In contrast, the proliferation of Hela cells was severely inhibited by N-PMNCs@DOX after incubation with for 6, 12, and 24 h (Figure 5). The cells cocultured with N-PMNCs@DOX for 6, 12, and 24 h displayed significantly lower ($p < 0.05$ or $p < 0.01$) cell viability than that of control. The phenomenon could be interpreted that the endocytosed DOX released from N-PMNCs@DOX in response to acidic condition at endosome/lysosome within cells and simultaneously killed cells.

Second, we investigated cell uptake and intracellular distributions of PMNCs and N-PMNCs. Hela cells were collected and observed by TEM and confocal laser scanning microscopy (CLSM) after incubation with PMNCs and N-PMNCs for 24 h. Intracellular endosomes (dash circles) were observed in Hela cells incubated with both PMNCs and N-PMNCs (Figure 6 A, left and right). However, we found that the endocytosed amount of N-PMNCs was higher than that of PMNCs via a CLSM observation (Figure 6 B, dark dots). Moreover, the endocytosed amounts of PMNCs and N-PMNCs were quantified by measuring the gray values of images via software of image pro plus 6.0. Cells treated with N-PMNCs displayed significantly higher ($p < 0.01$) gray value than those of PMNCs (see Figure S3 in the Supporting Information), indicating that more N-PMNCs were uptaken by Hela cells. The result suggests that the decoration with hydrazide improved the internalization efficiency of N-PMNCs. The potential mechanism is proposed as follows: first, the positively charged hydrazide was favorable for physical absorption of N-PMNCs onto negatively charged cell membranes;[39] second, the good dispersion of hydrophilic N-PMNCs in cell medium could promoted the cellular uptake of N-PMNCs.

As we know that exogenous substances could transport into cells through several different pathways including phagocytosis, endocytosis etc. To investigate the cellular endocytosis mechanism of N-PMNCs system, energy-dependent and pharmacological inhibitors mediated endocytosis were characterized. As for energy-dependent endocytosis, Hela cells were incubated with N-PMNCs@FITC at different conditions.[26] In control group, cells were incubated with N-PMNCs@FITC at 37 °C for 2 h; In the second group, cells were initially treated with sodium azide for 1 h, after that N-PMNCs@FITC were added and incubated for another 1 h; in the third group, cells were cocultured with N-PMNCs@FITC, however, at a low temperature of 4 °C for 2 h, respectively. Sodium azide is an agent that blocks the formation of adenosine 5-triphosphate (ATP) within cells. While the low temperature of 4 °C maintains the energy metabolism of cells at a low level.[40,41] The normalized fluorescence intensity of cells either treated with sodium azide or

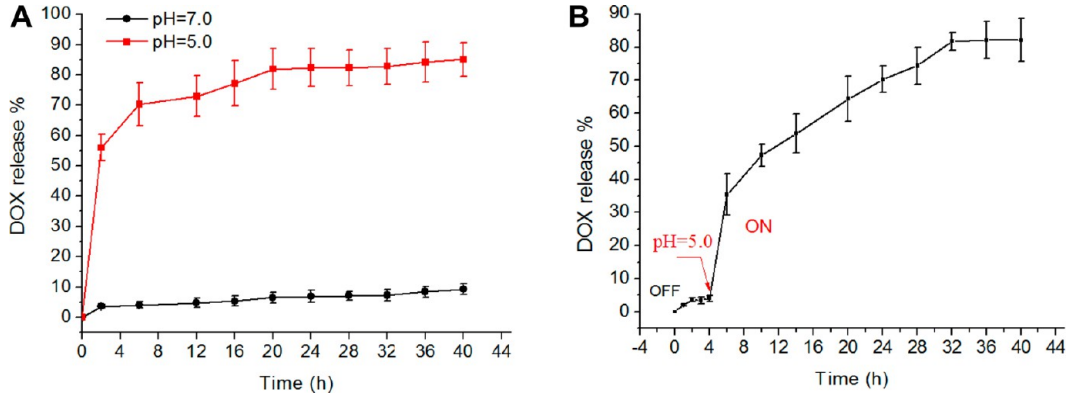

Figure 4. (A) In vitro DOX release profiles of N-PMNCs@DOX at pH 7.0 and 5.0, respectively (n = 5); (B) delayed release profiles of DOX from N-PMNCs@DOX in response to pH change after incubation for 4 h (n = 5).

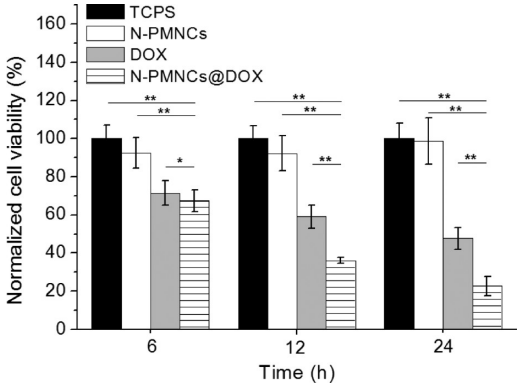

Figure 5. Cell viability of Hela cells treated with N-PMNCs, DOX and N-PMNCs@DOX (n = 6), *p < 0.05, **p < 0.01. Cell viability of cells cultured onto TCPS at each time of interval was employed as standard for normalization.

low temperature of 4 °C were only 51.6% and 21.3%, respectively (Figure 6 C), which were significantly lower than that of control (p < 0.01). The results directly indicate that the cell uptake of N-PMNCs system was an energy-dependent process. Moreover, pharmacological inhibitors (amiloride-HCl, amantadine-HCl and genistein) mediated cell uptake of N-PMNCs system were evaluated. Genistein, an inhibitor of caveolae-mediated cell uptake, displayed a small effect on the endocytosis of N-PMNCs system.[42] Amiloride-HCl, an inhibitor of macropinocytosis, led to around 19.3% reduction in cell uptake efficiency of N-PMNCs system.[43] Amantadine-HCl, an inhibitor of clathrin-mediated endocytosis, also significantly reduced the cell uptake of N-PMNCs system (Figure 6D).[44] There was significant difference in fluorescence intensity between the genistein treated cells and control (p < 0.05), whereas the cells treated both with amiloride-HCl and amantadine-HCl displayed significantly lower (p < 0.01) fluorescence intensity than that of control. The results suggest that N-PMNCs were uptaken mainly through macropinocytosis- and clathrin-mediated endocytosis pathways.

To further investigate the amount of N-PMNCs@DOX endocytosed by Hela cells at different time of intervals, we introduced N-PMNCs@FITC to replace N-PMNCs@DOX because of he cytotoxicity of DOX. After coculture with N-PMNCs@FITC for 6 h, around 27.4% of N-PMNCs@FITC was endocytosed by Hela cells. The endocytosed amount of N-PMNCs@FITC increased to 82.8% after incubation for 24 h (Figure 6E). The result suggests that the cell uptake is a time-dependent process.

Third, we investigated cell apoptosis induced by N-PMNCs, DOX, and N-PMNCs@DOX. CLSM was employed to observe the morphology of cell nuclei in this study. Hela cells cultured onto TCPS showed intact oval shape cell nuclei (Figure 7A, a1−a3). Cells treated with N-PMNCs displayed similar nuclei feature to those cultured onto TCPS and the number of cell increased steadily along with culture time increasing (Figure 7A, b1−b3). When Hela cells directly exposed to pure DOX, the cell nuclei appeared deformed and crush after incubation for 12 and 24 h because of its severe toxicity (Figure 7A, c1−c3), indicating that serious cell apoptosis and death. Similar phenomenon was also observed for Hela cells treated with N-PMNCs@DOX (Figure 7A, d1−d3). For cell apoptosis assay, we observed the apoptosis bodies through three-dimensional reconstruction of CLSM images from cells treated with N-PMNCs@DOX. The result again confirmed that DOX could efficiently release from N-PMNCs@DOX in cells endosomes/lysosomes and resulted in cell apoptosis (Figure 7B).

Fourth, to further confirm our hypothesis, we performed animal experiment to evaluate the antitumor efficiency of N-PMNCs@DOX in vivo. Four groups of nude mice bearing Hela tumor model with four mice in each group were intravenous injected for cancer therapy. To establish the tumor model, 2×10^6 Hela cells were subcutaneously injected into the left leg armpits of nude mice. After the tumor size reached approximately 50−60 mm^3, saline, DOX, N-PMNCs@DOX alone and N-PMNCs@DOX with magnetic field were injected via the tail veins every 3 days for 3 weeks, the magnetic field was applied at the tumor site for 2 h after every injection (see Figure S4 in the Supporting Information).

To confirm N-PMNCs@DOX could be efficiently targeted to tumor tissue with an external magnetic field, T2-weighted MR scanning was performed to track the locations of drug carriers in nude mice.[45,46] No magnetic signal in tumor tissue was observed before injection (Figure 8A, left). When no magnetic field was applied, only a weak dark signal was observed after injection of N-PMNCs@DOX for 9 days (Figure 8A, right, arrow). The accumulation of N-PMNCs@DOX could be contributed to the EPR effect.[10] In contrast, when a magnetic field (1.21 T) was applied, a large amount of dark signals could be observed at the tumor tissue after injection of N-PMNCs@DOX for 9 days (Figure 8B, right, arrows). In addition, a large amount of N-PMNCs@DOX were observed at the histological section of tumor tissue after applying magnetic field with Perls' Prussian blue staining, whereas only a small amount of N-PMNCs@DOX was observed without magnetic field treatment, which was also

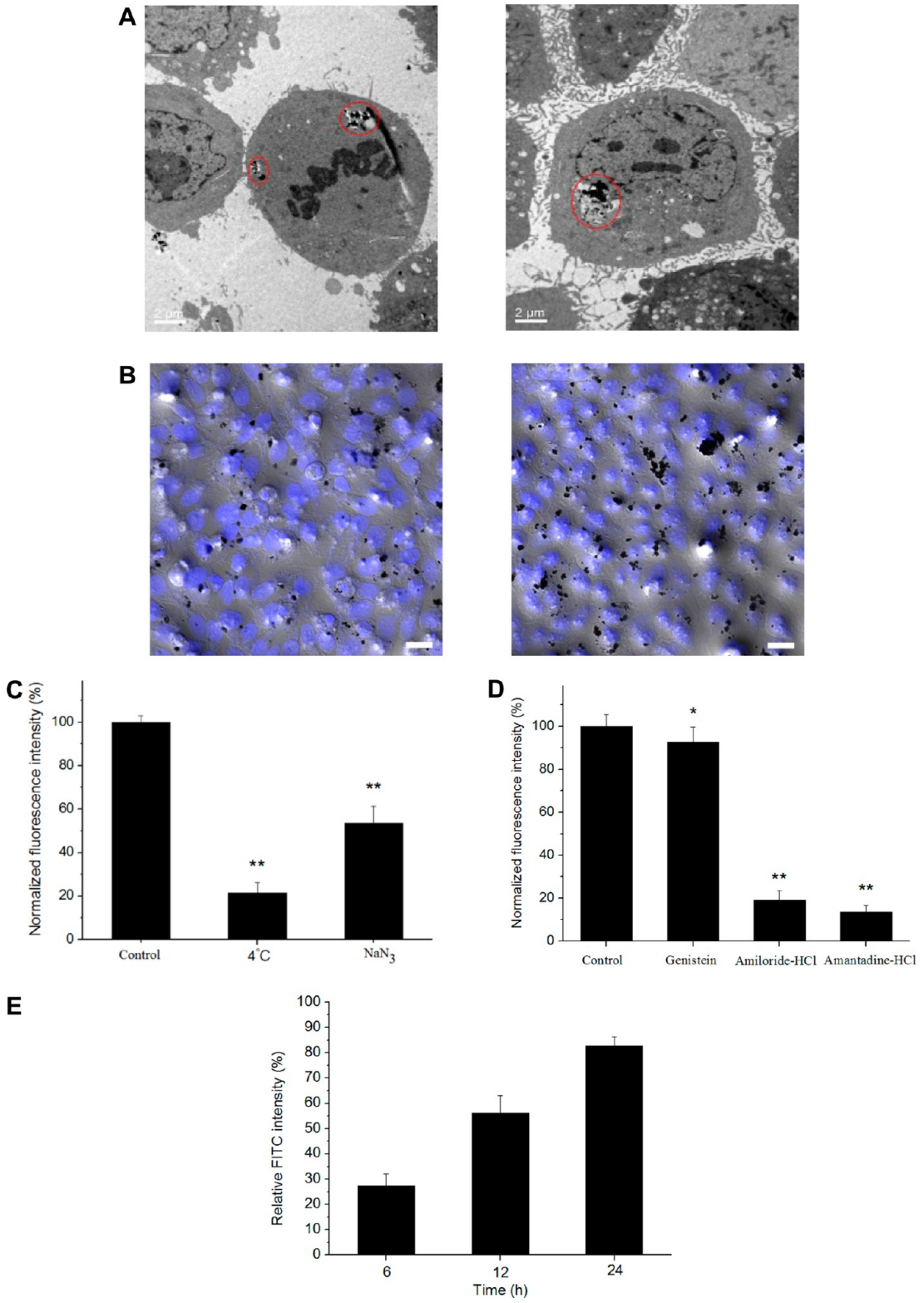

Figure 6. (A) TEM images of intracellular distribution of the internationalized PMNCs (left) and N-PMNCs (right); (B) CLSM images of cell uptake after incubating 24 h with PMNCs (left) and N-PMNCs (right); (C) energy-dependent cell uptake of N-PMNCs@FITC after culture for 1 h; (D) cell uptake of N-PMNCs@FITC by Hela cells pretreated with genistein, amiloride-HCl and amantadine-HCl for 1 h (right). ($n = 6$), $^{*}p < 0.05$, $^{**}p < 0.01$ vs control; and (E) relative FITC intensity of N-PMNCs@FITC endocytosed by Hela cells after culture for 6, 12, and 24 h ($n = 5$), respectively.

contributed to the EPR effect in solid tumor tissue (Figure 8 C left vs right). These results suggest that N-PMNCs@DOX could be efficiently targeted to tumor tissue by magnetic field for local drug delivery and N-PMNCs could be employed as an ideal contrast agent for MRI.

To evaluate antitumor efficiency and tumor necrosis, the tumor size was measured and histologically evaluated with TUNEL staining assay and hematoxylin-eosin (H&E) staining. Notable antitumor efficacy could be observed in the tumor tissue treated with (mag) N-PMNCs@DOX after therapy for 21 days

dx.doi.org/10.1021/am500818m | ACS Appl. Mater. Interfaces 2014, 6, 7395−7407

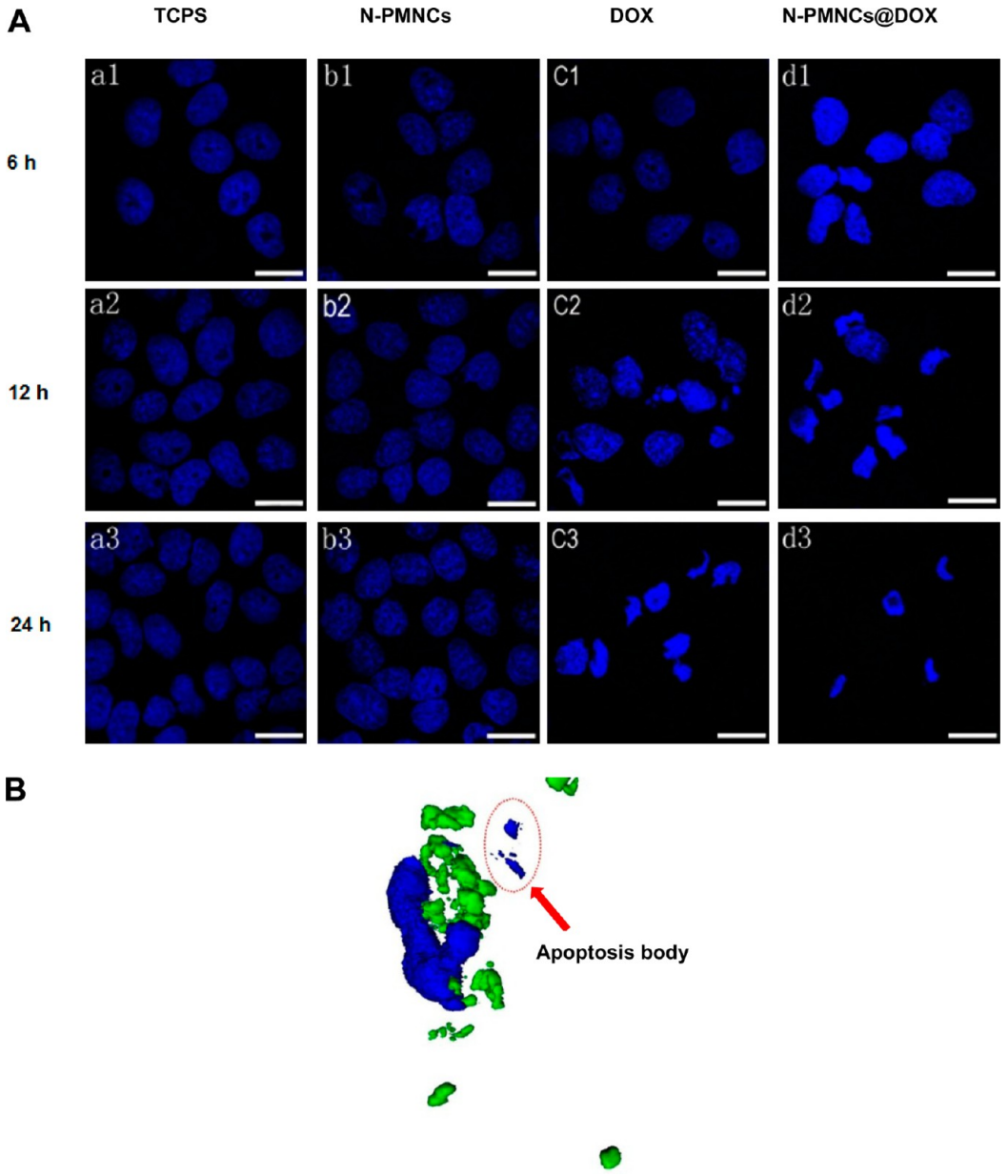

Figure 7. (A) Representative CLSM images of (a1−a3) TCPS, (b1−b3) N-PMNCs, (c1−c3) DOX, and (d1−d3) N-PMNCs@DOX after culture for 6, 12, and 24 h (scale bar: 20 μm). Blue: cell nuclei. (B) Three-dimensional reconstruction image of apoptosis body.

(Figure 9A). As shown in Figure 9B, no obvious difference in tumor sizes was observed in between four groups after the first injection. However, significant difference could be noticed between N-PMNCs@DOX with magnetic field group [(mag)N-PMNCs@DOX] and other three groups after the second injection (the sixth day). With respect to antitumor efficiency, DOX showed limited effect on the inhibition of tumor growth, mainly due to its hydrophobic property and short blood circulation time.[10] As we know that most antitumor drugs currently used in the clinic, such as DOX, camptothecin, and paclitaxel etc., are inherently hydrophobic, which limits their solubility in physiological fluids to kill tumor cells in a form of free drug. Thus, drug delivery carrier is essentially important for transport those drugs into tumor cells. Once a pH-responsive drug carrier is uptaken by tumor cells, the weak acidic microenvironment of tumor tissue or acidic lysosome/endosome would result in the drug release from the drug carrier, leading to local high concentration of antitumor drug within tumor tissue or tumor cells. It in turn diffuses into tumor cells' nuclei, leading to cell apoptosis or death.[7,10] In addition, N-PMNCs@DOX without magnetic field also showed moderate antitumor efficacy since only a limited amount of N-PMNCs@DOX could be delivered to tumor tissue. At the end of therapy, the tumors growth treated with (mag) N-PMNCs@DOX were heavily inhibited. The volumes of tumors in statistics were smaller than that of native tumors (0 day) even after feeding for 21 days (Figure 9B). The nude mice treated with (mag)N-PMNCs@DOX displayed a significantly smaller ($p < 0.01$) tumor volumes than that of saline (control). The results indicate that (mag)N-PMNCs@DOX could effectively inhibit the growth of tumor.

The TUNEL staining assays indicated that tumor treated with (mag) N-PMNCs@DOX induced extensive apoptosis of tumor cells (red). Besides, H&E staining of tumor slices showed that most tumor cells in tumor tissue had been killed when treated

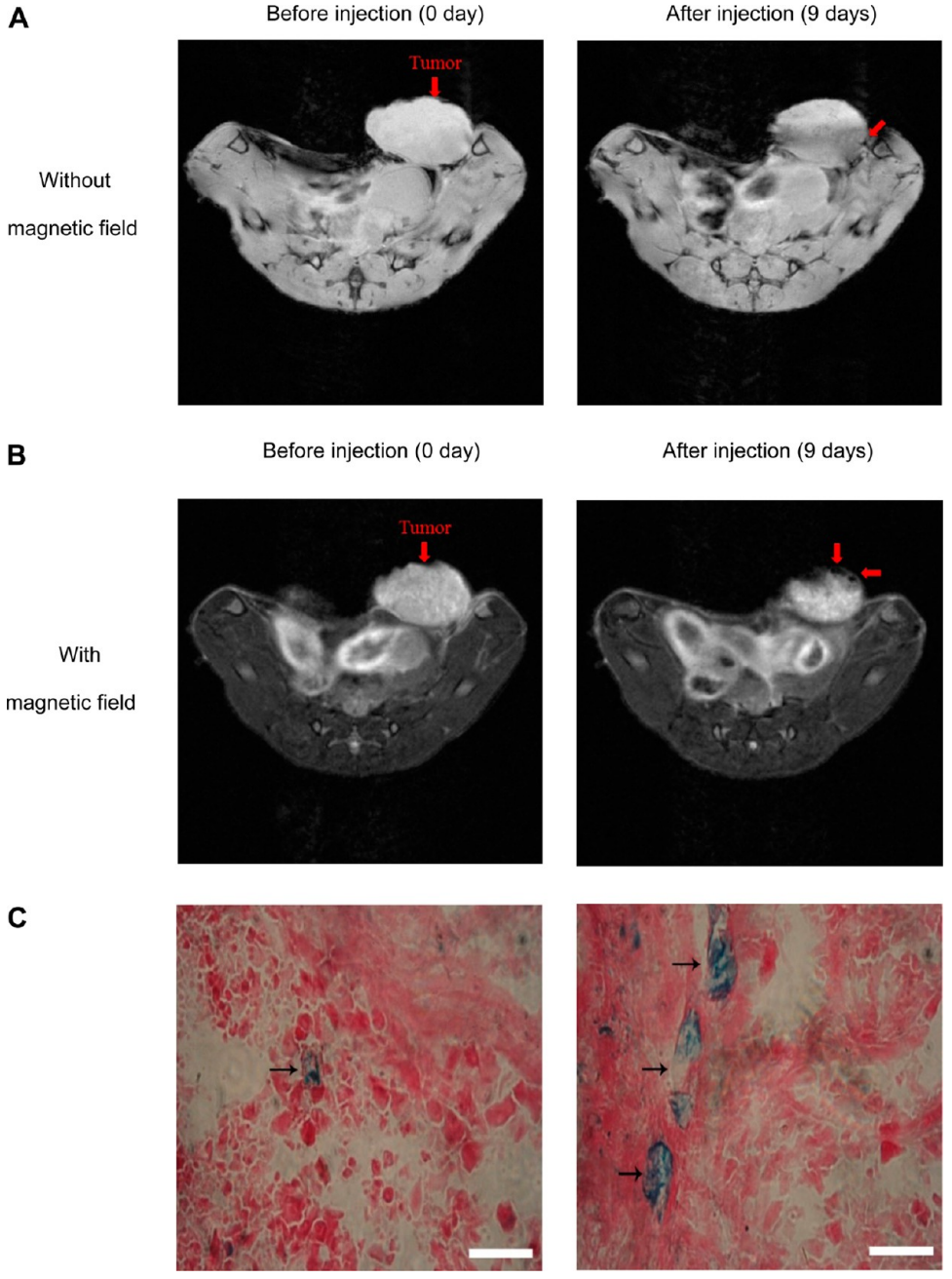

Figure 8. In vivo T2-weighted MR images of tumor before (left) and after (right) N-PMNCs@DOX was intravenously injected into nude mice for 9 days (A) without magnetic field and (B) with magnetic field treatment, respectively; and (C) images of Perls' Prussian blue stained tumor slices of nude mice treated with N-PMNCs@ DOX (left) and (Mag) N-PMNCs@DOX (right), respectively (scale bar: 200 μm).

with (mag) N-PMNCs@DOX; while other groups showed normal cell morphology (Figure 9C).[45] This result was consistent with the growth curve of tumor volume, further confirming that the therapy of N-PMNCs@DOX applied with magnetic field could efficiently inhibited tumor growth in vivo.

To evaluate toxic side effects of the drug delivery system, the weight of nude mice were monitored and major organs were stained by H&E for evaluation. It was observed that the weight of mice treated with saline, N-PMNCs@DOX only and N-PMNCs@DOX with magnetic field increased normally. However, for those mice treated with free DOX, their weights sharply decreased, even resulting in death after feeding for 21 days (Figure 10A). There was significant difference regarding weight of mice between DOX treatment and other treatments ($p < 0.01$).

Histological analysis of organs also indicated that severe toxicity was observed in heart and liver of the mice treated with free DOX (Figure 10B). In detail, the heart showed prominent cardiotoxicity presented with acute inflammatory cells (arrows). Besides, the liver toxicity induced by DOX demonstrated in forms of extensive nuclear shrinkage and inflammatory cells (arrows). These toxicities, in particular of the irreversible cardiotoxicity, were the dominant and direct reasons to induce the death of mice when treated with free DOX.[47,48] In contrast, other groups did not appear noticeable toxicity in major organs. It suggests that N-PMNCs@DOX could be applied for in vivo cancer therapy with limited side effects. The reason lies in that only limited N-PMNCs@DOX could be delivered to the normal tissue due to the linear blood vessels with smooth and intact

dx.doi.org/10.1021/am500818m | ACS Appl. Mater. Interfaces 2014, 6, 7395−7407

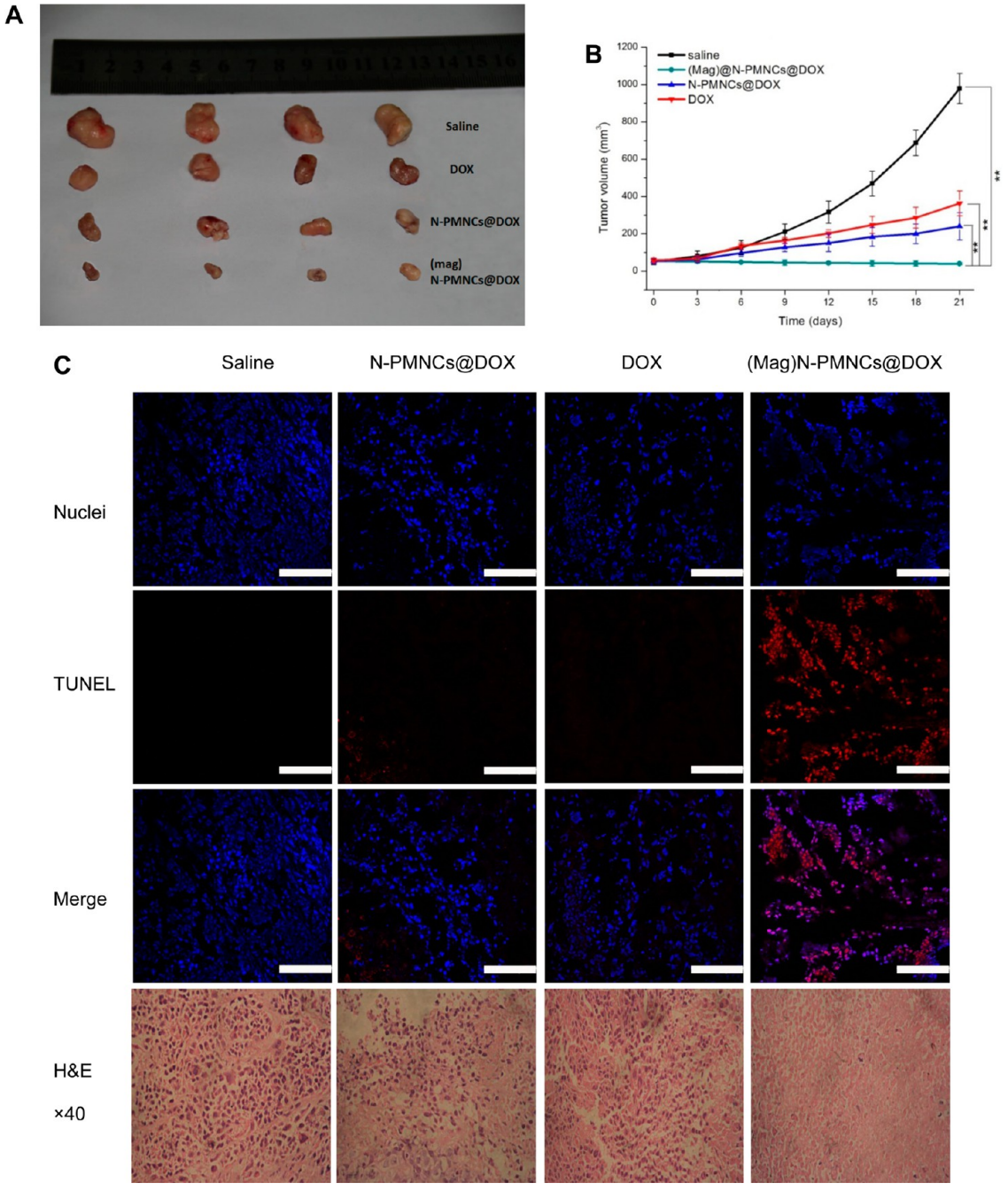

Figure 9. (A) Optical photos of tumors collected from all mice after treatments for 21 days; (B) in vivo tumor growth curves of mice with different treatments ($n = 4$) $^{**}p < 0.01$; and (C) TUNEL and H&E stained tumor slices of mice with different treatments (scale bar: 100 μm).

structure maintaining by pericytes in normal tissue,[49] which highly diminishes the EPR effect (commonly occurs at tumor tissue). It thus reduced the toxic side effects of DOX and improved biosafety of the system for in vivo application. Taken together, we confirmed our hypothesis that the fabricated N-PMNCs@DOX system could be employed as intracellular pH-responsive drug delivery in vitro and remotely targeted for tumor inhibition in vivo.

CONCLUSION

In summary, we fabricated a biocompatible, pH-responsive drug delivery system based on hydrazide bearing PMMA coated MNCs, DOX (model drug) was then covalently linked to PMMA via hydrazone bonds. The prepared N-PMNCs@DOX system demonstrated high pH-sensitivity for intracellular drug delivery in vitro. Furthermore, the magnetic nanocubes, as the core of nanocarrier, could be utilized to remotely targeted drug delivery via an external magnetic field *in vivo*. More importantly, the magnetically targeted drug delivery system of N-PMNCs@DOX enhanced the efficiency for tumor growth inhibition and reduced toxic side effects of chemotherapy in vivo. The N-PMNCs@DOX demonstrated great potential to be a promising carrier for efficient drug delivery in cancer therapy.

EXPERIMENTAL SECTION

Materials. $FeCl_3 \cdot 6H_2O$ was provided by Alfa Aesar Co (Tianjin, China). Sodium oleate, 1-octadecene, and fluorescence isothiocyanate were purchased from Aladdin Co (Shanghai, China). Oleic acid, ethanol, hexane, methyl methacrylate (MMA), methanol, sodium lauryl benzene

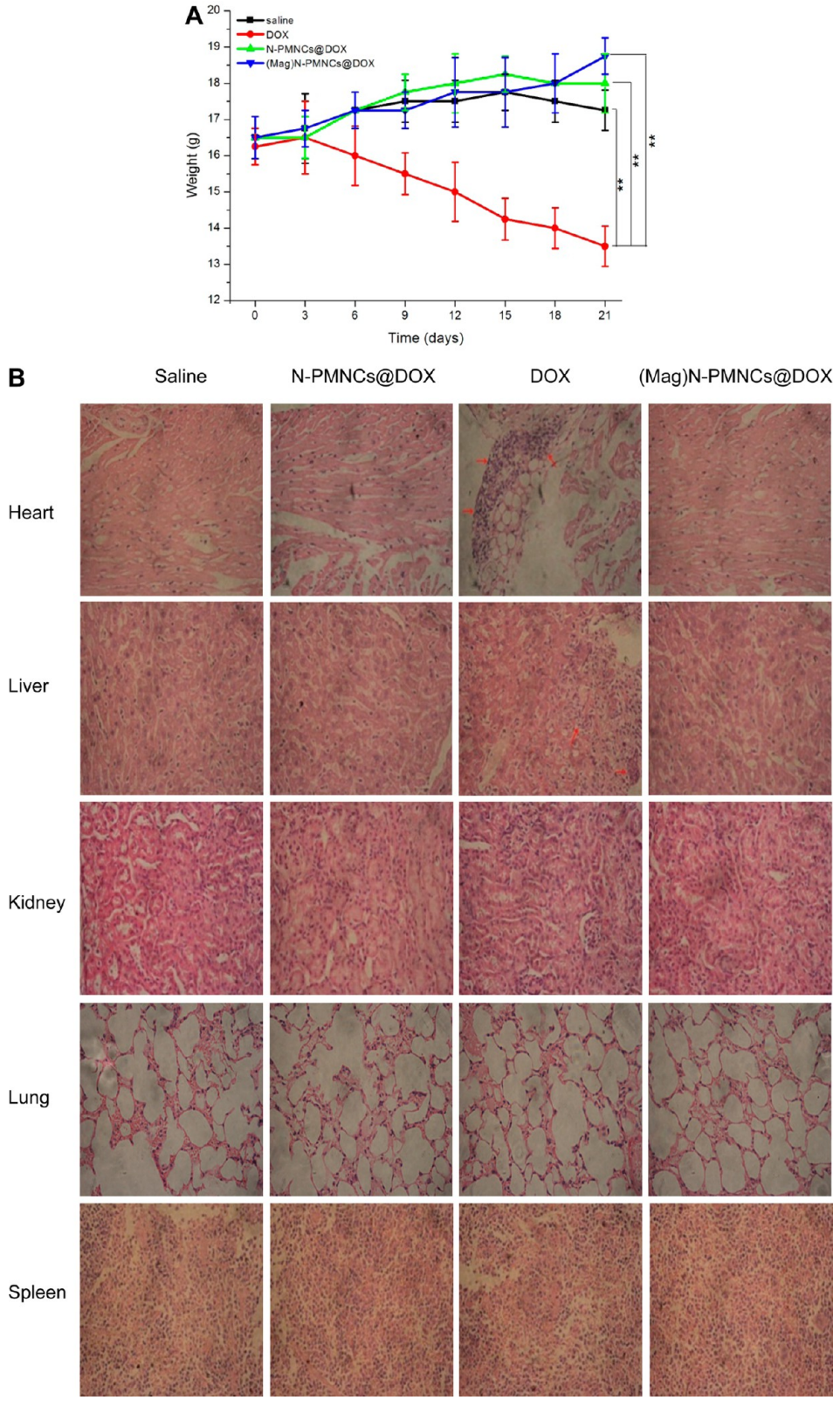

Figure 10. (A) Body weights of mice with different treatments ($n = 4$) $^{**}p < 0.01$; and (B) representative H&E staining images of the major organs of mice with different treatments (magnification 40×).

sulfate, hydrazine hydrate, trifluoroacetic acid (TFA), triethylamine (TEA), glutaraldehyde, paraformaldehyde, formalin, sodium azide, amantadine-HCl, amiloride-HCl, and genistein were provided by Oriental Chemical Co (Chongqing, China). Doxorubicin (DOX) and cell counting assay kit-8 were provided by Huake Chemical Co (Chongqing, China). Triton X-100 and Hoechst 33258 were supplied by Sigma Co. (St. Louis, MO, USA).

Synthesis of Magnetic Nanocubes. Magnetic nanocubes were synthesized with a thermal decomposition method.[32] Briefly, iron-oleate complex was first prepared by reacting metal chlorides with sodium

oleate. $FeCl_3 \cdot 6H_2O$ (10.8 g, 40 mmol) and sodium oleate (36.5 g, 120 mmol) were dissolved into mixture solution of 80 mL of ethanol, 60 mL of distilled water, and 140 mL of hexane. The mixture solution was heated to 70 °C and kept for 4 h. After the reaction was completed, the upper organic layer containing iron-oleate complex was washed with 30 mL of distilled water for 10 times in a separator funnel. The organic layer was then collected and dried in vacuum overnight. After hexane was evaporated off, the iron-oleate complex was collected in a waxy solid form. Subsequently, 36 g of iron−oleate complex and 5.7 g of oleic acid were dissolved in 200 mL of 1-octadecene at room temperature. The mixture solution was heated to 380 °C at a constant heating rate of 3.3 °C min^{-1}, and then kept at 380 °C for 30 min. After that, the resulting solution was cooled down to room temperature and 500 mL of ethanol was added. The precipitation was the iron oxide nanocubes. Finally, the nanocubes were separated by centrifugation and washed with ethanol for 10 times. The iron oxide nanocubes were dried in a vacuum overnight and kept in a desiccator.

Preparation of PMMA-Coated Magnetic Nanocubes (PMNCs). PMMA coated magnetic nanocubes were prepared via an aqueous-phase radical polymerization.[33] Typically, 200 mg of magnetic nanocubes was dispersed into 50 mL ethanol in a three-necked round-bottom flask with sonication for 10 min. Then, 50 mL of aqueous solution containing 10 mg of sodium lauryl benzene sulfate was added under mechanically stirring at room temperature for 1 h. Next, 1 g of MMA monomer was added and the resultant dispersion was bubbled with nitrogen for 0.5 h. Subsequently, the flask was heated to 70 °C for polymerization with vigorous agitation for 24 h. The resulting nanocubes were washed with ethanol and distilled water each for 3 times. The PMMA-coated magnetic nanocubes were dried in vacuum at 50 °C for 10 h.

Synthesis of Hydrazide-PMNCs (N-PMNCs) and Loading of DOX. The N-PMNCs was synthesized according to previous studies through conversing methyl esters to hydrazine bonds with hydrazine hydrate.[50] Briefly, PMNCs (3 g) and hydrazine hydrate (10 g) was dissolved into methanol (50 mL) and refluxed at room temperature for 12 h. The precipitate was then washed with distilled water 5 times and freeze-dried. DOX was conjugated to the N-PMNCs through the formation of hydrazone bonds.[23] Briefly, N-PMNCs (50 mg) were dissolved into 20 mL of anhydrous methanol containing 10 mg of DOX. Then, 5 μL of TFA and 100 μL of TEA was added and the mixture solution was bubbled with nitrogen for 10 min and was stirred in dark at room temperature for 24 h. After that, the precipitant was washed with anhydrous methanol and distilled water each for 10 times, respectively, until no absorbance at 480 nm was detected in the supernatant via an UV−vis spectrophotometer (Lambda 900, PerkinElmer, USA). The precipitant was then freeze-dried. After loading with DOX, the precipitant was washed with anhydrous methanol for 15 times, until no absorbance was detected from the supernatant by UV−vis spectrophotometer. The washed anhydrous methanol were collected and added to the initial solvent. The mixed solvent was then detected via a UV−vis spectrophotometer at a wavelength of 480 nm. The amount of DOX in supernatant could be calculated from a standard calibration curve of DOX. The loading efficiency of N-PMNCs@DOX was calculated from the following equation[36,38]

$$\text{drug loading efficiency (\%)} = \left[1 - \frac{\text{drug in supernatant liquid}}{\text{total drug added}}\right] \times 100 \quad (1)$$

Characterizations. The morphologies and particle sizes of MNCs and PMNCs were observed by using transmission electron microscopy (TEM, Hitachi-7500, Hitachi, Japan). Fourier transform infrared spectra (FTIR, model 6300, Bio-Rad Co. Ltd., USA), magnetic hysteresis loops (VSM, Lake Shore 7410, Germany), and thermogravimetric analysis (Micromeritics Co, USA) were employed to analyze the physical properties of MNCs, N-PMNCs and N-PMNCs@DOX, respectively. Enzyme linked immunosorbent assay (ELISA, model 689, Bio-Rad Co. Ltd., USA) was employed to analyze the cytotoxicity of different magnetic nanocubes. Cells morphologies and cell apoptosis were observed by confocal laser scanning microscopy (CLSM, LSM 510 Metanlo, Zeiss Co., Germany). Caliper was employed to measure the size of tumor. TUNEL stained assay was observed by CLSM. Perls' Prussian blue staining and H&E staining were observed by fluorescence microscope.

In Vitro DOX Release Study. In vitro DOX release was measured by UV−vis spectrophotometer. To reduce the analytical system error, N-PMNCs@DOX was equally divided into 10 portions and each portion (10 mg) was dispersed into 5 mL of phosphate buffer saline (PBS) with different pH values of 7.4 and 5.0 in a conical tube. These tubes were incubated at 37 °C with shaking. After incubation for a specific time of interval, 1 mL of supernatant liquid was taken out for measurement, while adding another 1 mL fresh PBS in the tube. The absorbance of the released DOX was measured with a UV−vis spectrophotometer at a wavelength of 480 nm. In addition, another 5 portions were dispersed into 5 mL of PBS with pH 7.4 for 4 h, and then the pH value of PBS was adjusted to 5.0 and incubated for another 36 h. The absorbance of DOX was measured as the same manner above. The release percentage of DOX was calculated according to a DOX calibration curve. DOX release from N-PMNCs@DOX was calculated from the following equation

$$\text{DOX release}(\%) = (I_t - I_0)/(I_\infty - I_0) \times 100 \quad (2)$$

where I_0 is the initial fluorescence intensity of samples without incubation; I_t is the fluorescence intensity of samples after incubation for a desired time; and I_∞ is the fluorescence intensity of samples with ultrasonic treatment at pH 2.0 for 48 h, i.e., the total loading amount of DOX.

Cell Culture. Human cervical carcinoma HeLa cell line was kindly provided by Professor Lin Chen from Radiology department of Daping Hospital (Chongqing). Cells were cultured with DMEM (High Glucose) medium containing 10% fetal bovine serum (FBS, Gibco), 100 U/mL of penicillin, and 100 μg/mL streptomycin at 37 °C under a 5% CO_2 atmosphere. The culture medium was changed every 2 days.

Cytotoxicity Assay. The effect of DOX on the proliferation of Hela cells was evaluated by a cell counting assay kit-8 (CCK-8). Hela cells were seeded into 24-well plates at an initial cell density of 2×10^4 cells/cm^2. When cell confluence reached around 60−70%, the culture medium was replaced with fresh media containing N-PMNCs, DOX or N-PMNCs@DOX (DOX equivalent, 40 μg/mL DOX). Hela cells were further incubated at 37 °C for another 6, 12, and 24 h, respectively. Then, 10 μL of CCK-8 solution was added to each well and the cells were incubated at 37 °C for another 2 h. Finally, the culture medium was collected in a 96-well plate and measured with enzyme linked immunosorbent assay (ELISA) at a wavelength of 450 nm.

Cell Uptake Assay. Hela cells were seeded into cell culture flasks at an initial cell density of 2×10^4 cells/cm^2. When cell confluence reached around 60−70%, the culture medium was replaced with fresh media containing PMNCs or N-PMNCs at a concentration of 40 μg/mL. After incubation at 37 °C for another 12 h, the cells were digested by 0.25% trypsin-EDTA and washed by PBS. The cells were fixed by 2.5% glutaraldehyde for 24 h and observed by TEM (Hitachi-7500, Hitachi, Japan) and confocal laser scanning microscopy (CLSM). The amount of PMNCs or N-PMNCs endocytosed by Hela cells was quantified by calculating the gray value via a software of image pro plus 6.0 ($n = 6$).

Cell Uptake Mechanism Assay. To investigate the cell uptake mechanism,[26] N-PMNCs was loaded with fluorescence isothiocyanate (FITC) through the reaction of isothiocyanate with amino groups of N-PMNCs. Briefly, N-PMNCs (50 mg) were added into 20 mL of PBS (pH 7.4) containing 10 mg of FITC and stirred in dark at room temperature for 24 h. After that, the precipitant was washed with PBS 10 times. Hela cells were seeded to 24-well plate at an initial cell density of 2×10^4 cells/cm^2 and allowed to reach cell confluence of 60−70%. Then, Hela cells were treated as follows: first, Hela cells were cultured with N-PMNCs@FITC for 2 h either at 37 °C (control) or 4 °C. Another group of cells were culture at 37 °C after pretreated with sodium azide for 1 h. The excessive nanoparticles were removed by washing with PBS 3 times. Cells were lysed by 0.1% Triton-X100. Then, the cell lysate was collected to measure the fluorescence intensity via a fluorescence spectrophotometer; second, different pharmacological inhibitors, including amantadine-HCl (1 mM), amiloride-HCl (2.5 mM), and genistein (100 mM), were utilized to treat Hela cells for

1 h before incubation with N-PMNCs@FITC. After culture for another 2 h, cells were lysed for fluorescence intensity assay as mentioned above.

Cell Apoptosis Assay. Hela cells were cultured with N-PMNCs, DOX or N-PMNCs@DOX in 35 mm × 12 mm cell culture dish (NEST Biotechnology Co., LTD, China) at 37 °C in the same manner as above-mentioned. After incubation at 37 °C for another 6 h, 12 and 24 h, the plate was washed with PBS for 3 times. The cells were then fixed by 2% paraformaldehyde at 4 °C for 25 min and washed with PBS for 3 times. Next, 0.2% Triton X-100 was added and kept at 4 °C for 2 min. Subsequently, cell nuclei were stained with 10 μg/mL Hoechst 33258 (Sigma) for 5 min. Finally, the stained samples were mounted with 90% glycerinum. Cell nuclei were observed with a CLSM.

Endocytosis Percentage Assay. To investigate the percentage of N-PMNCs@DOX endocytosed by cells, we used N-PMNCs@FITC because of the cytotoxicity of DOX. N-PMNCs@FITC endocytosed by cells was evaluated by measuring the fluorescence intensity of FITC. Hela cells were cultured with 1.1 mg/mL N-PMNCs@FITC at 37 °C for 6, 12, and 24 h, respectively. Next, the treated cells were washed with PBS 3 times to remove excessive N-PMNCs@FITC which were not endocytosed. Then, the cells was collected in tubes and dispersed into 5 mL of PBS (pH 7.4) after being digested by trypsin. After that, 0.1% Triton X-100 was added and kept at 4 °C for 30 min to lyse Hela cells. The cell lysate was collected to measure the fluorescence intensity via a fluorescence spectrophotometer. The percentage of endocytosed N-PMNCs@FITC was calculated from the following equation

$$\text{endocytosed N-PMNCs@FITC (\%)} = F_t/F_0 \times 100 \quad (3)$$

where F_t is the fluorescence intensity of samples after incubation for a desired time; F_0 is the fluorescence intensity of the added N-PMNCs@FITC.

Animal Model. All animal procedures were performed according to the protocol approved by the Institutional Animal Care and Use Committee of China. Female nude mice of 4−6 weeks old (weight 16−17 g) were purchased from Animal laboratory of Xinqiao Hospital. Nude mice were subcutaneously injected in the left limb armpits with 100 μL of a cell suspension containing 2×10^6 Hela cells. When tumor reached approximately 50−60 mm^3, the tumor-bearing mice (n = 4/group) were injected via the tail veins with saline, free DOX, N-PMNCs@DOX alone, or N-PMNCs@DOX (DOX equivalent, 2 mg/kg DOX) with magnetic field once every 3 days.

The body weights of mice were recorded, the tumor size was estimated by caliper measurement before every injection. The tumor volume was calculated as $V_{tumor} = ab^2/2$, where a and b are the maximum and minimum diameters, respectively.[51,52] The T2-weighted MR images were obtained before injection and after (9 days) injection of N-PMNCs@DOX by a 7.0 T Magnetic Resonance Imaging (BioSpec 70/20USR, Bruker, Germany). After feeding for 3 weeks, all mice were euthanized and sacrificed, tumors and organs of heart, liver, spleen, lung and kidney were separated. The tumors and organs were washed by PBS and stored in 4% formalin solution at 4 °C for 48 h. The treated organs were then embedded in paraffin and the slices were finally stained with hematoxylin-eosin (H&E). The tumor sections were stained with Perls' Prussian blue for the observation of the injected magnetic nanocubes and TUNEL staining assay for detecting DNA stands breakage by apoptosis.

Statistical Analysis. All data were expressed as means ± standard deviations (SD). The statistical analysis was performed using Student's t test and one-way analysis of variance (ANOVA) at confidence levels of 95 and 99% (OriginPro version 7.5).

■ ASSOCIATED CONTENT

Supporting Information

Other supplementary data. This material is available free of charge via the Internet at http://pubs.acs.org.

■ AUTHOR INFORMATION

Corresponding Author

*E-mail: kaiyong_cai@cqu.edu.cn.

Author Contributions

The manuscript was written through contributions of all authors. All authors have given approval to the final version of the manuscript.

Notes

The authors declare no competing financial interest.

■ ACKNOWLEDGMENTS

This work was financially supported by Natural Science Foundation of Chongqing Municipal Government (CSTC, 2011JJJQ10004), Natural Science Foundation of China (21274169 and 31200712), Fundamental Research Funds for the Central Universities (Project CDJZR 10238801) and the "111" project (B06023).

■ REFERENCES

(1) Das, S.; Ranjan, P.; Maiti, P.; Singh, G.; Leitus, G.; Klajn, R. Dual-Responsive Nanoparticles and Their Self-assembly. *Adv. Mater.* **2013**, *25*, 422−426.

(2) Ding, X.; Cai, K.; Luo, Z.; Li, J.; Shen, X. Biocompatible Magnetic Liposomes for Temperature Triggered Drug Delivery. *Nanoscale* **2012**, *4*, 6289−6292.

(3) Luo, Z.; Cai, K.; Hu, Y.; Zhao, L.; Liu, P.; Duan, L.; Yang, W. Mesoporous Silica Nanoparticles End-Capped with Collagen: Redox-Responsive Nanoreservoirs for Targeted Drug Delivery. *Angew. Chem., Int. Ed.* **2011**, *50*, 640−643.

(4) Pan, L.; He, Q.; Liu, J.; Chen, Y.; Zhang, L.; Shi, J. Nuclear-Targeted Drug Delivery of TAT Peptide-Conjugated Monodisperse Mesoporous Silica Nanoparticles. *J. Am. Chem. Soc.* **2012**, *134*, 5722−5725.

(5) Jang, H.; Ryoo, S.-R.; Kostarelos, K.; Han, S. W.; Min, D. H. The Effective Nuclear Delivery of Doxorubicin from Dextran-Coated Gold Nanoparticles Larger than Nuclear Pores. *Biomaterials* **2013**, *34*, 3503−3510.

(6) Park, H.; Tsutsumi, H.; Mihara, H. Cell Penetration and Cell-Selective Drug Delivery Using α-helix Peptides Conjugated with Gold Nanoparticles. *Biomaterials* **2013**, *34*, 4872−4879.

(7) Brannon-Peppas, L.; Blanchette, J. O. Nanoparticle and Targeted Systems for Cancer Therapy. *Adv. Drug. Delivery Rev.* **2012**, *64*, 206−212.

(8) Yin, M.; Li, Z.; Liu, Z.; Ren, J.; Yang, X.; Qu, X. Photosensitizer-Incorporated G-Quadruplex DNA-Functionalized Magnetofluorescent Nanoparticles for Targeted Magnetic Resonance/Fluorescence Multimodal Imaging and Subsequent Photodynamic Therapy of Cancer. *Chem. Commun.* **2012**, *48*, 6556−6558.

(9) Zhou, L.; Li, Z.; Liu, Z.; Ren, J.; Qu, X. Luminescent Carbon Dot-Gated Nanovehicles for Ph-Triggered Intracellular Controlled Release and Imaging. *Langmuir* **2013**, *29*, 6396−6403.

(10) Fang, J.; Nakamura, H.; Maeda, H. The EPR Effect: Unique Features of Tumor Blood Vessels for Drug Delivery, Factors Involved, and Limitations and Augmentation of The Effect. *Adv. Drug Delivery Rev.* **2011**, *63*, 136−151.

(11) Jiang, L.; Zhou, Q.; Mu, K.; Xie, H.; Zhu, Y.; Zhu, W.; Zhao, Y.; Xu, H.; Yang, X. pH/temperature Sensitive Magnetic Nanogels Conjugated with Cy5.5-labled Lactoferrin for MR and Fluorescence Imaging of Glioma in Rats. *Biomaterials* **2013**, *34*, 7418−7428.

(12) Li, X.; Li, H.; Liu, G.; Deng, Z.; Wu, S.; Li, P.; Xu, Z.; Xu, H.; Chu, P. K. Magnetite-Loaded Fluorine-Containing Polymeric Micelles for Magnetic Resonance Imaging and Drug Delivery. *Biomaterials* **2012**, *33*, 3013−3024.

(13) Bae, K. H.; Park, M.; Do, M. J.; Lee, N.; Ryu, J. H.; Kim, G. W.; Kim, C.-G.; Park, T. G.; Hyeon, T. Chitosan Oligosaccharide-Stabilized Ferrimagnetic Iron Oxide Nanocubes For Magnetically Modulated Cancer Hyperthermia. *ACS Nano* **2012**, *6*, 5266−5273.

(14) Lee, N.; Choi, Y.; Lee, Y.; Park, M.; Moon, W. K.; Choi, S. H.; Hyeon, T. Water-Dispersible Ferrimagnetic Iron Oxide Nanocubes with

Extremely High r_2 Relaxivity for Highly Sensitive in Vivo MRI of Tumors. *Nano Lett.* **2012**, *12*, 3127−3131.
(15) Arun, T.; Prakash, K.; Kuppusamy, R.; Justin Joseyphus, R. Magnetic Properties of Prussian Blue Modified Fe_3O_4 Nanocubes. *J. Phys. Chem. Solids* **2013**, *74*, 1761−1768.
(16) Mo, R.; Sun, Q.; Xue, J.; Li, N.; Li, W.; Zhang, C.; Ping, Q. Multistage pH-Responsive Liposomes for Mitochondrial-Targeted Anticancer Drug Delivery. *Adv. Mater.* **2012**, *24*, 3659−3665.
(17) Wang, W.; Cheng, D.; Gong, F.; Miao, X.; Shuai, X. Design of Multifunctional Micelle for Tumor-Targeted Intracellular Drug Release and Fluorescent Imaging. *Adv. Mater.* **2012**, *24*, 115−120.
(18) Rocha, U.; Jacinto da Silva, C.; Ferreira Silva, W.; Guedes, I.; Benayas, A.; Martínez Maestro, L.; Acosta Elias, M.; Bovero, E.; van Veggel, F. C.; García Solé, J. A.; Jaque, D. Subtissue Thermal Sensing Based on Neodymium-Doped LaF3 Nanoparticles. *ACS Nano* **2013**, *7*, 1188−1199.
(19) Katherine, J. M.; Matthew, B. F. Recyclable Thermoresponsive Polymer−Cellulase Bioconjugates for Biomass Depolymerization. *J. Am. Chem. Soc.* **2013**, *135*, 293−300.
(20) Coll, C.; Mondragón, L.; Martínez-Máñez, R.; Sancenón, F.; Marcos, M. D.; Soto, J.; Amorós, P.; Pérez-Payá, E. Enzyme-Mediated Controlled Release Systems by Anchoring Peptide Sequences on Mesoporous Silica Supports. *Angew. Chem., Int. Ed.* **2011**, *50*, 2138−2140.
(21) Aimetti, A. A.; Machen, A. J.; Anseth, K. S. Poly(Ethylene Glycol) Hydrogels Formed by Thiol-Ene Photopolymerization for Enzyme-Responsive Protein Delivery. *Biomaterials* **2009**, *30*, 6048−6054.
(22) He, H.; Chen, S.; Zhou, J.; Dou, Y.; Song, L.; Zhou, X.; Chen, X.; Jia, Y.; Li, S.; Li, X. Cyclodextrin-Derived pH-Responsive Nanoparticles for Delivery of Paclitaxel. *Biomaterials* **2013**, *34*, 5344−5358.
(23) Wang, F.; Pauletti, G. M.; Wang, J.; Zhang, J.; Ewing, R. C.; Wang, Y.; Shi, D. Dual Surface-Functionalized Janus Nanocomposites of Polystyrene/Fe_3O_4@SiO_2 for Simultaneous Tumor Cell Targeting and Stimulus-Induced Drug Release. *Adv. Mater.* **2013**, *25*, 3485−3489.
(24) Chen, H.; Moore, T.; Qi, B.; Colvin, D. C.; Jelen, E. K.; Hitchcock, D. A.; He, J.; Mefford, O. T.; Gore, J. C.; Alexis, F.; Anker, J. N. Monitoring pH-Triggered Drug Release from Radioluminescent Nanocapsules with X-ray Excited Optical Luminescence. *ACS Nano* **2013**, *7*, 1178−1187.
(25) Soppimath, K. S.; Tan, D. W.; Yang, Y. pH-Triggered Thermally Responsive Polymer Core-Shell Nanoparticles for Drug Delivery. *Adv. Mater.* **2005**, *17*, 318−323.
(26) Luo, Z.; Cai, K.; Hu, Y.; Zhang, B.; Xu, D. Cell-Specific Intracellular Anticancer Drug Delivery from Mesoporous Silica Nanoparticles with pH Sensitivity. *Adv. Healthcare Mater.* **2012**, *1*, 321−325.
(27) Ghosh, A.; Haverick, M.; Stump, K.; Yang, X.; Tweedle, M. F.; Goldberger, J. E. Fine-Tuning The pH Trigger of Self-Assembly. *J. Am. Chem. Soc.* **2012**, *134*, 3647−3650.
(28) LaVan, D. A.; McGuire, T.; Langer, R. Small-Scale Systems for in Vivo Drug Delivery. *Nat. Biotechnol.* **2003**, *21*, 1184−1191.
(29) Vijayakumar, S.; Adithya, A.; Kalluraya, B.; Sharafudeen, K. N.; Chandrasekharan, K. Study of Third-Order Optical Nonlinearities of Substituted Hydrazones in PMMA. *Appl. Polym. Sci.* **2011**, *119*, 595−601.
(30) Ge, J.; Neofytou, E.; Lei, J.; Beygui, R. E.; Zare, R. N. Protein−Polymer Hybrid Nanoparticles for Drug Delivery. *Small* **2012**, *8*, 3573−3578.
(31) Lan, F.; Hu, H.; Jiang, W.; Liu, K.; Zeng, X.; Wu, Y.; Gu, Z. Synthesis of Superparamagnetic Fe_3O_4/PMMA/SiO_2 Nanorattles with Periodic Mesoporous Shell for Lysozyme Adsorption. *Nanoscale* **2012**, *4*, 2264−2267.
(32) Park, J.; An, K.; Hwang, Y.; Park, J.-G.; Noh, H.-J.; Kim, J.-Y.; Park, J.-H.; Hwang, N.-M.; Hyeon, T. Ultra-Large-Scale Syntheses of Monodisperse Nanocrystals. *Nat. Mater.* **2004**, *3*, 891−895.
(33) Chen, H.; Deng, C.; Zhang, X. Synthesis of Fe_3O_4@SiO_2@PMMA Core−Shell−Shell Magnetic Microspheres for Highly Efficient Enrichment of Peptides and Proteins for MALDI - ToF MS Analysis. *Angew. Chem., Int. Ed.* **2010**, *49*, 607−611.
(34) Kim, D.; Lee, N.; Park, M.; Kim, B. H.; An, K.; Hyeon, T. Synthesis of Uniform Ferrimagnetic Magnetite Nanocubes. *J. Am. Chem. Soc.* **2009**, *131*, 454−455.
(35) Fritsch, E. Static and Fatigue Properties of Two New Low-Viscosity Pmma Bone Cements Improved by Vacuum Mixing. *J. Biomed. Mater. Res.* **1996**, *4*, 451−456.
(36) Pan, Y.-J.; Chen, Y.-Y.; Wang, D.; Wei, C.; Guo, J.; Lu, D.-R.; Chu, C.-C.; Wang, C.-C. Redox/pH Dual Stimuli-Responsive Biodegradable Nanohydrogels with Varying Responses to Dithiothreitol and Glutathione for Controlled Drug Release. *Biomaterials* **2012**, *33*, 6570−6579.
(37) Jonas, U.; Shah, K.; Norvez, S.; Charych, D. H. Reversible Color Switching and Unusual Solution Polymerization of Hydrazide-Modified Diacetylene Lipids. *J. Am. Chem. Soc.* **1999**, *121*, 4580−4588.
(38) Dora, C. P.; Singh, S. K.; Kumar, S.; Datusalia, A. K.; Deep, A. Development and Characterization of Nanoparticles of Glibenclamide by Solvent Displacement Method. *Acta Polym. Pharm.* **2010**, *3*, 283−290.
(39) Hu, Y.; Cai, K.; Luo, Z.; Hu, Y.; Cai, K.; Luo, Z. Construction of Polyethyleneimine - β - Cyclodextrin/pDNA Multilayer Structure for Improved in Situ Gene Transfection. *Adv. Eng. Mater.* **2010**, *12*, B18−B25.
(40) Chae, S.; Kim, H.; Lee, M. S.; Jang, Y. L.; Lee, Y.; Lee, S. H.; Lee, K.; Kim, S. H.; Kim, H. T.; Chi, S.-C.; Park, T. G.; Jeong, J. H. Energy-Independent Intracellular Gene Delivery Mediated by Polymeric Biomimetics of Cell-Penetrating Peptides. *Macromol. Biosci.* **2011**, *11*, 1169−1174.
(41) Iversen, T.; Skotland, T.; Sandvig, K. Endocytosis and Intracellular Transport of Nanoparticles: Present Knowledge and Need for Future Studies. *Nano Today* **2011**, *6*, 176−185.
(42) Koivusalo, M.; Welch, C.; Hayashi, H.; Scott, C. C.; Kim, M.; Alexander, T.; Touret, N.; Hahn, K. M.; Grinstein, S. Amiloride Inhibits Macropinocytosis by Lowering Submembranous Ph and Preventing Rac1 and Cdc42 Signaling. *J. Cell. Biol.* **2010**, *188*, 547−563.
(43) Perry, D.; Daugherty, G.; Martin, W. Clathrin-Coated Pit-Associated Proteins Are Required for Alveolar Macrophage Phagocytosis. *J. Immunol.* **1999**, *162*, 380−386.
(44) Iwasa, A.; Akita, H.; Khalil, I.; Kogure, K.; Futaki, S.; Harashima, H. Cellular Uptake and Subsequent Intracellular Trafficking of R8-Liposomes Introduced at Low Temperature. *BBA-Biomembranes.* **2006**, *1758*, 713−720.
(45) Wang, C.; Xu, H.; Liang, C.; Liu, Y.; Li, Z.; Yang, G.; Cheng, L.; Li, Y.; Liu, Z. Iron Oxide @ Polypyrrole Nanoparticles As A Multifunctional Drug Carrier for Remotely Controlled Cancer Therapy with Synergistic Antitumor Effect. *ACS Nano* **2013**, *7*, 6782−6795.
(46) Hwang, D. W.; Song, I. C.; Lee, D. S.; Kim, S. Smart Magnetic Fluorescent Nanoparticale Imaging Probes to Monitor MicroRNAs. *Small* **2010**, *6*, 81−88.
(47) Meng, H.; Xue, M.; Xia, T.; Ji, Z.; Tarn, D. Y.; Zink, J. I.; Nel, A. E. Use of Size and A Copolymer Design Feature to Improve The Biodistribution and The Enhanced Permeability and Retention Effect of Doxorubicin-Loaded Mesoporous Silica Nanoparticles in A Murine Xenograft Tumor Model. *ACS Nano* **2011**, *5*, 4131−4144.
(48) Kalaria, D.; Sharma, G.; Beniwal, V.; Ravi Kumar, M. N. Design of Biodegradable Nanoparticles for Oral Delivery of Doxorubicin: in Vivo Pharmacokinetics and Toxicity Studies in Rats. *Pharm. Res.* **2009**, *26*, 492−501.
(49) Danhier, F.; Olivier, F.; Véronique, P. To Exploit the Tumor Microenvironment: Passive and Active Tumor Targeting of Nanocarriers for Anti-Cancer Drug Delivery. *J. Controlled Release* **2010**, *148*, 135−146.
(50) Zhao, X.; Wang, X.; Jiang, X.; Chen, Y. Q.; Li, Z. T.; Chen, G. J. Hydrazide-Based Quadruply Hydrogen-Bonded Heterodimers, Structure, Assembling Selectivity, and Supramolecular Substitution. *J. Am. Chem. Soc.* **2003**, *125*, 15128−15139.
(51) Tomayko, M. M.; Reynolds, C. P. Determination of Subcutaneous Tumor Size in Athymic (nude) Mice. *Cancer. Chemother. Pharm.* **1989**, *24*, 148−154.
(52) Euhus, D. M.; Hudd, C.; Laregina, M. C.; Johnson, F. E. Tumor Measurement in The Nude Mouse. *J. Surg. Oncol.* **1986**, *31*, 229−234.